Basic mechanisms of Frenkel pair recombinations in UO_2 fluorite structure calculated by molecular dynamics simulations

L. Van Brutzel* and A. Chartier
CEA, DEN, Serv Phys Chem, F-91191 Gif-sur-Yvette, France

J. P. Crocombette
CEA, DEN, Serv Rech Met Phys, F-91191 Gif-sur-Yvette, France
(Received 25 February 2008; published 15 July 2008)

In the present paper, the analysis of Frenkel pair recombinations is investigated by empirical-potential–molecular dynamics simulations. Frenkel pairs with separation distance between the vacancy and the interstitial up to 1.5 times the lattice parameter have been studied. For each Frenkel pair, their lifetimes as a function of the temperature and their migration paths are analyzed. For both uranium and oxygen defects, the picture of the recombination is rather complex and depends on the separation distance and the structure. A thermal dependence on the recombination lifetimes is found in separation distance larger than 7 Å. The energy that an interstitial must overcome to recombine with a vacancy is lower than the migration energy of the diffusion. This recombination activation energy is also related to the pathways of the vacancy hops during the recombinations. Recombination distances are discussed and compared with the results from previous displacement cascade simulations. Finally, the role of Frenkel pair recombinations on the resistance to amorphization in UO_2 is discussed.

DOI: 10.1103/PhysRevB.78.024111 PACS number(s): 61.72.Cc, 61.80.Az, 66.30.hd

I. INTRODUCTION

Uranium dioxide (UO_2) is the most common ceramic used as nuclear fuel in the present nuclear industry. Understanding its behavior under irradiation or self-irradiation is then of great interest for the design and the safety of both nuclear plants and direct storage repositories. In spite of an extensive number of experimental studies as well as theoretical works, the complete understanding of its behavior under radiation is still not fully clear. It is well known that the fluoritelike UO_2 matrix resists even for high doses to amorphization.[1–3] However, the basic mechanisms for this tolerance are yet to be clarified. For instance, in the broader framework of the ceramics, there exist several theories to explain the resistance to amorphization. Some authors are relating this resistance to chemical bond effects[4] or topology[5] and structural effects,[6] while others are pointing out the kinetics of point defects[7] and, more specifically, the crucial role of Frenkel pair (FP) recombinations.[8] Herein, we will address the last point, i.e., FPs recombination, with respect to UO_2.

Computational modeling such as molecular dynamics (MD) provides, at the atomic scale, good insights into the nature and the behavior of defects generated during irradiation. Previous empirical-potential MD simulations of displacement cascades in UO_2 with energies up to 80 keV[9,10] show no amorphization of the fluorite matrix even if, during the cascade, part of the simulation box is melted. At the end of cascades, the primary damage state consists mainly of vacancies located in the cascade's core and interstitials distributed at the periphery of the subcascade branches. Those defects form stable FPs at the time scale of the simulation (few picoseconds).

However, the fast recovery stage, i.e., the fast recombination of defects created during the displacement cascades, has not yet been studied in detail. Moreover, it is known that fast recombination of close metastable FPs plays a major role in this fast recovery stage.[11] Besides, recent works in pyrochlore fluoritelike structure[8,12] show that the complex recombination of the cation FPs can explain the amorphous transition of the matrix. In this paper, we will focus on the study of the FP recombinations in UO_2 up to a separation distance between the vacancy and the interstitial equal to 1.5 times the conventional lattice parameter a_0. Because recombination has been shown to be a thermally activated process,[11] the FP lifetimes are studied as a function of temperature. The recombination activation energies for this process are compared with the diffusion migration energies. For each recombination, a migration path is found and will be discussed. Finally, the role of FP recombination on the resistance to amorphization is discussed and compared with previous work done in lanthanum zirconate pyrochlore.

This paper is organized as follows: in Sec. II the computational procedure is described; in Sec. III the results of the uranium and oxygen FP recombinations are presented; finally, in Sec. IV on the basis of the results, the recombination mechanism is discussed.

II. COMPUTATIONAL PROCEDURE

The MD calculation was performed using a Born-Mayer-Huggins-type potential for the repulsive part coupled with a full Ewald summation to describe the Coulomb interactions. The analytical function of the potential is defined as

$$V_{\alpha\beta}(r_{ij}) = A_{\alpha\beta}\exp\left(-\frac{r_{ij}}{B_{\alpha\beta}}\right) - \frac{C_{\alpha\beta}}{r_{ij}^6} + \frac{z_\alpha z_\beta}{4\pi\epsilon_0 r_{ij}}, \qquad (1)$$

where A, B, and C are adjustable parameters, r_{ij} is the distance between the atoms i and j, Z is the ionic partial charge, and α and β design the type of atom. Details of the potential

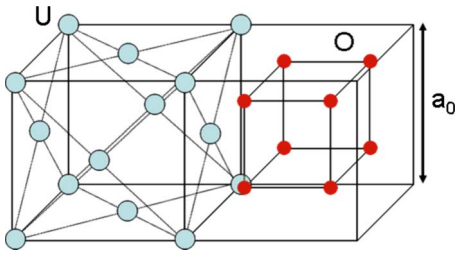

FIG. 1. (Color online) Schematic representation of the fluorite structure with a lattice parameter a_0.

parameters and its validation were reported by Morelon *et al.*[13] elsewhere. However, it is important to point out that this interatomic potential has been designed to best reproduce the formation and migration energies of uranium and oxygen point defects (vacancy, interstitial, and FP). Moreover, comparison of other pair empirical potentials has been reported by Govers *et al.*[14] They calculated that the Morelon potential is one of the best concerning the point defect creation and migration energies. Periodic boundary conditions are used in all the three dimensions to prevent surface effects.

For a better understanding of the results presented in this paper, it is necessary to remember the fluorite structure, and to define properly the FP defects. The fluorite structure can be described as two embedded sublattices. The cation sublattice forms a faced-centered-cubic (fcc) lattice, and the anion sublattice forms a simple cubic (sc) lattice located at the tetrahedral sites of the cation fcc sublattice shown in Fig. 1. Each conventional fluorite unit cell consists of four uranium atoms and eight oxygen atoms.

A FP is defined as a pair of one interstitial and one vacancy on either the cation or anion sublattice. The interstitial positions for both cation and anion are located at the octahedral site of the fcc cation sublattice. It exists for the same separation distance, several interstitial positions possible for a given vacancy. To each distance, we will associate a specific FP rank starting by the closest. Namely, rank 1 corresponds to the lower distance between a vacancy and an interstitial. Tables I and II summarize the different FP ranks, their distances, and the number of possible interstitial positions for the fluorite structure up to about $3/2a_0$ (8.2 Å) for both uranium and oxygen vacancy, respectively. Figures 2 and 3 represent the positions of the different FPs possible in each sublattice. In both uranium and oxygen sublattices, for the distance corresponding to rank 4, there are two different types of FPs corresponding to two different symmetries noted in the following by rank 4 of type I and rank 4 of type II.

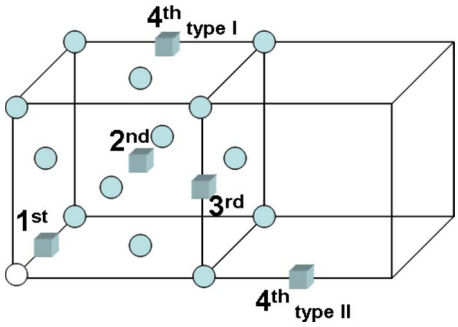

FIG. 2. (Color online) Schematic representation of the uranium sublattice and the different Frenkel pairs possible up to 8.08 Å. The full spheres represent the uranium atoms, the empty sphere represents the uranium vacancy, and the cubes represent the uranium interstitial positions.

To calculate the lifetime of a specific FP, a box of $3\times3\times3$ conventional unit cells of UO_2 in fluorite structure is relaxed under constant temperature (at the desired temperature), and at a constant pressure (0 GPa) during 20 ps. Then a FP is created by displacing an ion from its original lattice position to one of the interstitial positions located at the octahedral site of the fcc cation sublattice. After the creation of a FP, the system is relaxed for 1 ns under constant temperature. In order to preserve the accuracy of the trajectories, a variable time-step algorithm is used during the simulation. This variable time-step algorithm described by Delaye *et al.*[15] defines a means to increase or decrease gradually the time step based on the maximum kinetic energy found in the simulation box. The objective is to ensure that the fastest atom does not move farther than a fraction of an angstrom between two successive computational steps.

For some defect geometries, the FP survives for some time but the recombination takes place before the end of the simulation. This time is denoted in the following as the FP lifetime. In these cases, we also store the diffusion path of the recombination for analysis. As we shall see below, the surviving time of such a metastable pair decreases with temperature so that at low temperature, the recombination may be not achieved at the end of the simulated time (1 ns). In some other cases, the recombination does not take place irrespective of temperature. We arbitrarily define these configurations of defects as stable FPs. In order to improve the statistics for each FP rank, all the different interstitial positions in four different initial velocity configurations are analyzed. The range of the studied temperatures varies according to each case from 1 to 2500 K. The temperature never

TABLE I. Table summarizing the recombination data for the uranium FPs.

Rank	Distance [Å]	Number of possible interstitial	Recombination type	Times τ [ps]
1st	2.73	6	Instantaneous/Direct	<0.4 ps
2nd	4.73	8	None	No recombination
3rd	6.11	24	Instantaneous/Indirect	<1 ps
4th type I	8.2	24	Thermally activated/Indirect	$0.91\exp(0.64/k_BT)$
4th type II	8.2	24	Thermally activated/Indirect	$6.18\times10^{-2}\exp(1.31/k_BT)$

TABLE II. Table summarizing the recombination data for the oxygen FPs.

Rank	Distance [Å]	Number of possible interstitial	Recombination type	Times τ [ps]
1st	2.36	4	Instantaneous/Direct	<0.2 ps
2nd	4.53	12	Instantaneous/Indirect	<0.5 ps
3rd	5.95	12	Thermally activated/Indirect	$0.36\exp(0.16/k_BT)$
4th type I	7.1	16	Thermally activated/Indirect	$0.475\exp(0.058/k_BT)$
4th type II	7.1	4	Thermally activated/Indirect	$0.86\exp(0.21/k_BT)$
5th	8.08	24	Thermally activated/Indirect	$0.28\exp(0.27/k_BT)$

exceeded 2500 K in order to stay in the range of validity of the interatomic potential.

III. RESULTS

The lifetimes of the different uranium FP ranks are plotted using logarithmic scale against $1/k_BT$, where k_B is the Boltzmann constant and T is the temperature. The results are summarized in Fig. 4. The data points correspond to the results of the simulations within error bars due to the statistics, and the straight lines are the best fit using an Arrhenius function,

$$\tau = \tau_O \exp\left(\frac{E_a}{k_BT}\right), \tag{2}$$

where E_a is the recombination activation energy or energy barrier, which an interstitial must overcome to recombine with the vacancy, and τ_O is a pre-exponential factor, which is on the order of the inverse of the Debye frequency. The errors on the activation energies presented below are the standard deviations of the fit. One can see in Fig. 4 that the FP lifetime is very correctly fitted by this Arrhenius function. This proves that FP recombination is indeed a thermally activated process.

For the uranium FP of rank 1, corresponding to the smaller distance, the recombination is direct and instantaneous along the crystallographic direction [100] [see Fig. 5(a)]. The uranium atom in the interstitial position recombines for each temperature with a time inferior to 0.4 ps.

The uranium FP of rank 2 remains stable at the end of the simulations whatever the temperature. The limitation of the computational time to 1 ns may be too short to allow the occurrence of the recombination. Nonetheless, this lifetime is much higher than all the other ranks studied even for larger separation distances. One possible explanation for this stability is that in such configuration, to facilitate the migration of the uranium vacancy, the surrounding oxygen ions need to move away from the vacancy along the [111] crystallographic direction. In the case of the uranium FP of rank 2, the oxygen atom present along the [111] direction between the uranium interstitial and the vacancy is not free to move due to the presence of the interstitial. This configuration makes the vacancy hop along the direction [110] more energetically and prevents the recombination.

For the uranium FP of rank 3, we observe a very fast recombination within 1 ps by two successive replacements. This fast recombination is insensitive to the temperature. For the configuration shown in Fig. 5(b), the closest uranium atom along the crystallographic direction [100] from the interstitial recombines with the vacancy along the crystallographic direction [110]. Subsequently, the interstitial replaces this atom recombining with the new vacancy created. The full recombination process can be seen as vacancy diffusion with a subsequent instantaneous recombination of rank 1.

As presented in Sec. II, the FP of rank 4 has two types of symmetry. Each type recombines with a different path and with a different time scale. For type I, the recombination occurs with three successive replacements shown in Fig.

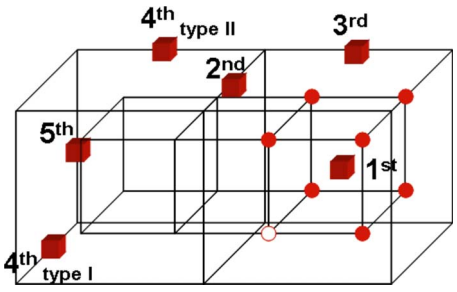

FIG. 3. (Color online) Schematic representation of the oxygen sublattice and the different FPs possible up to 8.2 Å. The full spheres represent the oxygen atoms, the empty sphere represents the oxygen vacancy, and the cubes represent the oxygen interstitial positions.

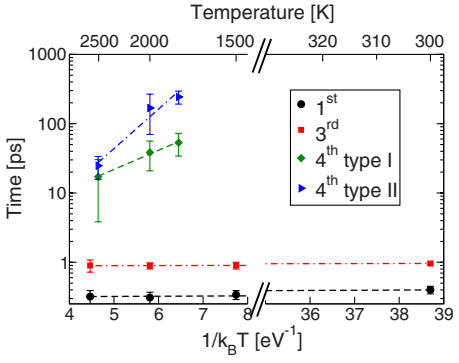

FIG. 4. (Color online) Lifetimes of the FP of ranks 1, 3, and 4 for different temperatures in an Arrhenius plot. The data points are the results of the simulations, and the straight lines are the best fits of Eq. (2). The graph has been cut in order to show the lifetime evolution over a larger scale for the FP of ranks 1 and 3. Rank 2 does not appear because for each temperature, it never recombines.

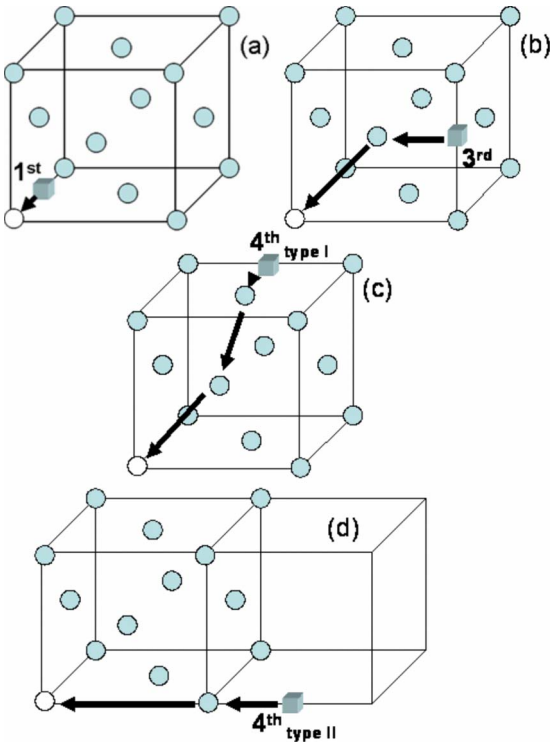

FIG. 5. (Color online) Schematic representations of the migration paths for the recombinations of the uranium FPs of ranks (a) 1, (b) 3, (c) 4 of type I, and (d) 4 of type II.

5(c): two hops of the vacancy along the crystallographic direction [110], and then a recombination along the crystallographic direction [100]. There are only two replacements for type II: a first hop of the vacancy along the crystallographic direction [100], and then a recombination along the same direction. Even if only three data points were found due to a computer time limitation, an Arrhenius plot can be calculated with activation energies equal to $0.64 \pm 5 \times 10^{-2}$ and 1.31 ± 0.28 eV for types I and II, respectively. All the results for the uranium FP recombination are summarized in Table I.

The same type of analysis is done for the recombination of the oxygen FPs. Figure 6 plots the lifetimes of the oxygen FPs in Arrhenius representation, and all the results for the oxygen FP recombinations are summarized in Table II.

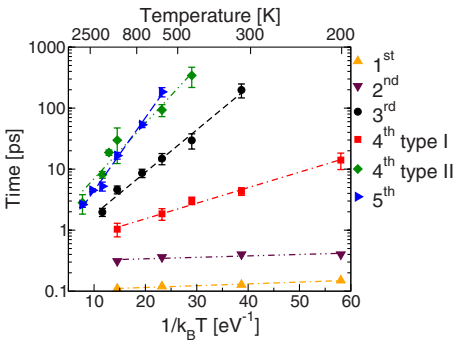

FIG. 6. (Color online) Lifetimes of the oxygen FPs of ranks 1, 2, 3, 4, and 5 for different temperatures in an Arrhenius plot. The data points are the results of the simulations, and the straight lines are the best fits of Eq. (2).

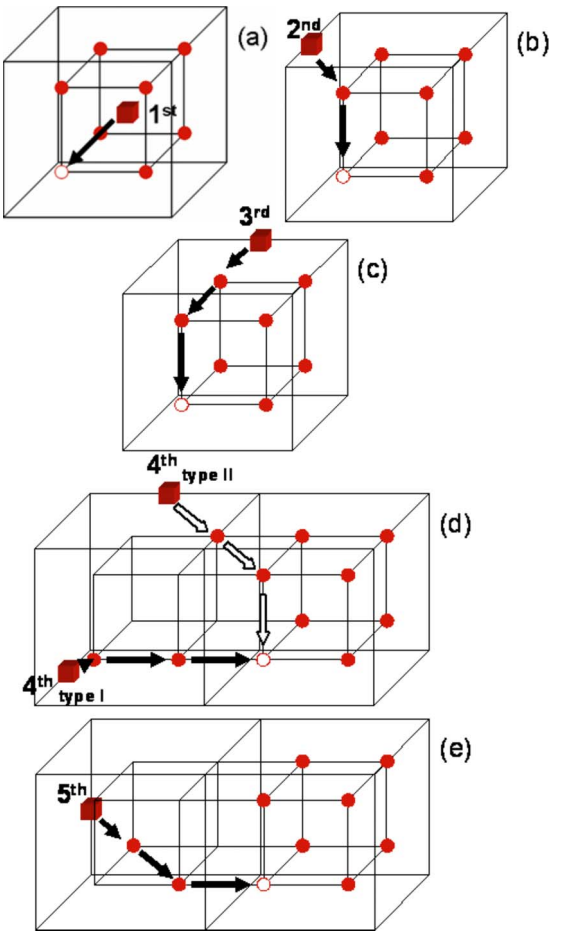

FIG. 7. (Color online) Schematic representations of the migration paths for the recombinations of the oxygen FP of ranks (a) 1, (b) 2, (c) 3, (d) 4, and (e) 5.

For the first two ranks, the lifetimes are insensitive to the evolution with the temperature. Indeed, the recombination is really fast, typically less than 0.2 and 0.5 ps, respectively, and can be considered as instantaneous. However, the migration paths are different. For rank 1 the recombination is direct along the crystallographic direction [111] as shown in Fig. 7(a). For rank 2 the recombination is indirect with a first hop of the vacancy along the crystallographic direction [100], followed by the recombination along the crystallographic direction [111] [see Fig. 7(b)].

For the superior ranks, there exists a significant dependence of the lifetimes with the temperature. It is interesting to point out that these lifetimes do not increase with the rank, namely, the separation distance between the interstitial and the vacancy. Indeed, the lifetimes of rank 4 in type I are lower than those of rank 3 with an activation energy equal to $0.058 \pm 3 \times 10^{-3}$ eV compared with $0.16 \pm 8 \times 10^{-3}$ eV for rank 3, whereas the lifetimes of ranks 4 of type II and 5 follow the same evolution with activation energies equal to $0.21 \pm 2 \times 10^{-2}$ and $0.27 \pm 1.3 \times 10^{-2}$ eV, respectively.

This behavior probably originates in the differences of the migration paths. Figure 7(c) shows the recombination path for the oxygen FP of rank 3. This recombination first takes place with two hops of the vacancy along the directions

[001] and [010] for this configuration, and then a recombination along the crystallographic direction [111]. For rank 4 of type I, it is almost the same path as rank 3, except the two hops of the vacancy are always done consecutively, with the same vector in the crystallographic direction [100] [see Fig. 7(d)]. The ranks 4 of type II and 5 have the same recombination sequence: a first hop of the vacancy along the crystallographic direction [100], followed by a second hop in the crystallographic direction [110], and then a recombination along the crystallographic direction [111]; see Figs. 7(d) and 7(e).

IV. DISCUSSION

The results presented in Sec. III exhibit different behaviors for the recombination of the FPs showing that the separation distance between the interstitial and the vacancy is not the only criterion that needs to be taken into account to determine the defect stability. In certain cases, the recombination mechanism is thermally activated. Using Arrhenius representation for the evolution of the FP lifetimes, activation energies which correspond to the energies to be overcome to obtain the recombination are found. It is then interesting to compare these energies with the migration energies found for the diffusion. In Fig. 8 are plotted the results of the oxygen diffusion coefficients calculated with the mean-square displacements of the oxygen atoms in a stoichiometric UO_2 matrix and in a hypostoichiometric $UO_{1.91}$ matrix (i.e., containing pre-existing vacancies). In these simulations, diffusion occurs only at high temperatures typically above 1000 K. With the presence of pre-existing vacancies, the oxygen diffusion is significantly accelerated. The migration energy drops from 2.94 eV for the stoichiometric case to 0.58 eV for the $UO_{1.91}$ matrix. The equivalent oxygen diffusion coefficients for the recombination of the oxygen FP of ranks 3 to 5 are plotted in Fig. 8 and expressed by the following equation:

$$D = \frac{d^2}{\tau_0}\exp(E_a/k_BT), \tag{3}$$

where d is the distance between the vacancy and the interstitial, τ_0 is the pre-exponential factor, and E_a is the activation energy or the energy barrier found in Sec. III. The diffusion coefficients are at least two orders of magnitude lower than the equivalent recombination diffusion for all the temperatures. Moreover, the activation energies for the recombinations are much lower than the defect migration energies (0.27 eV for the highest with rank 5, against 0.58 eV for the migration in $UO_{1.91}$). For the uranium atoms, no diffusion has been found even for matrices containing pre-existing uranium vacancies. Nevertheless, some recent *ab initio* simulations calculate the uranium vacancy migration energy equal to 4.4 eV (Ref. 16). This value is much higher than the highest activation energy for the recombination (1.31 eV for rank 4 in type II). These differences on the vacancy diffusion behavior for both uranium and oxygen atoms can be interpreted by the fact that the thermal diffusion is a pure random-walk process, whereas the diffusion by recombination is induced and directed by the presence of the second defect (interstitial).

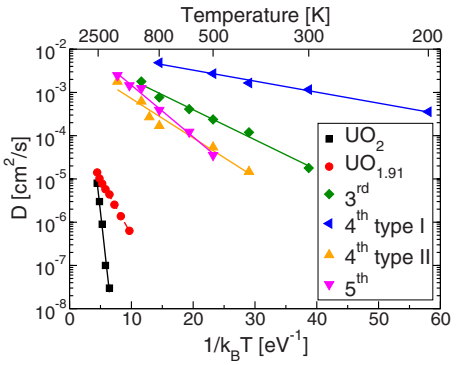

FIG. 8. (Color online) Arrhenius plots of the oxygen diffusion coefficients in UO_2 and $UO_{1.91}$ compared with the equivalent oxygen diffusion coefficients for the FP recombination.

Furthermore, no correlation exists between of the activation energy values and the separation distances between the interstitial and the vacancy. For the oxygen FP, the activation energy of rank 3 is higher than the activation energy of rank 4 in type I, and both of the ranks 4 do not have the same energies. This trend is also found for the uranium FP, where rank 2 has no recombination calculated, and both of the ranks 4 have different values. The value of the activation energy seems to depend on the structure, and more specifically on the sequence of the migration paths during the recombination.

We have described in Sec. III that the first stage of the recombination can be seen as a vacancy migration over several hops until the vacancy reaches a position corresponding to the FP of rank 1, in which case it recombines instantaneously. In all the cases presented in Sec. III, the number of hops is either one or two along various crystallographic directions. Here, one needs to be reminded that the interatomic model used in those simulations does not take into account the electronic structure, and then the change of charge associated on each atom, which probably occurs during the migration path. However, such a model was successful to predict the indirect migration of oxygen interstitial, which has been found to be energetically the most favorable path with the density functional theory (DFT) *ab initio* calculations.[16] Therefore, it is reasonable to suggest that in our model, the recombination mechanism corresponds to the shorter path, which includes the most favorable crystallographic directions for each sublattice. For the oxygen sublattice, the minimum for the activation energy is associated with hops in the crystallographic direction [100], whereas for the uranium sublattice, it is the direction [110] which yields to the minimum. This is in agreement with the *ab initio* calculations, which find that the migration energy for the oxygen vacancy in the direction [100] is less than half of the energy in the direction [110] (Ref. 16) (1.2 and 2.7 eV, respectively).

The simulations carried out here show that the global picture of the FP recombination mechanism in UO_2 is rather complex. It reveals thermal-activated processes, different from thermal diffusion, which depends partially on the separation distance between the interstitial, the vacancy, and the structure. This complexity has been also observed in other ceramics, such as pyrochlorelike structure ($La_2Zr_2O_7$) (Ref.

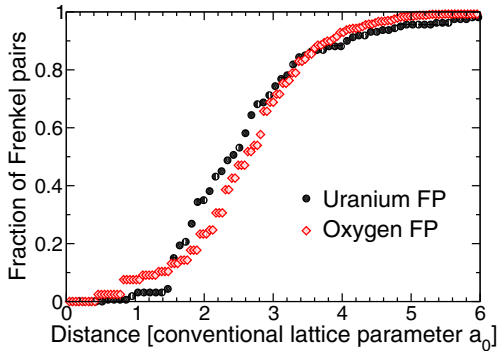

FIG. 9. (Color online) Integrated fraction of FPs as a function of their minimum separation distance after displacement cascades initiated with an energy of 80 keV.

12) and SiC (Refs. 17 and 18). However, in this last material, the authors were able to define two different recombination distances. We applied the same description to UO_2. In both sublattices, we can define a first "spontaneous recombination distance" r_{sd}, where the recombination is instantaneous (<1 ns) and which has no dependence on the temperature. It equals to about $r_{sd}=6/5a_0$ for the uranium FP (ranks 1 and 3), and to $r_{sd}=4/5a_0$ for the oxygen FP (ranks 1 and 2), where a_0 is the lattice parameter ($a_0=5.468$ Å at 300 K). A second, "thermal recombination distance" r_{td}, which involves thermal dependence of the recombination, is then defined. Because no higher distances than $3/2a_0$ for the FP separation distance have been tested, we can only define that the distance r_{td} is not lower than $3/2a_0$.

In previous studies,[9,10] it has been stated that the fast FP recombinations in UO_2 can explain the rapid reconstruction of the fluorite lattice during collision cascades. Therefore, another means to study the fast FP recombinations consists of investigating the FP configurations at the end of the cascades. The data of several displacement cascades initiated with an energy of 80 keV have been analyzed. For each vacancy, the closest interstitial is found, and this couple is then counted as one FP. The integrated fraction of FPs against their minimum separation distance is plotted in Fig. 9.

For both uranium FPs and oxygen FPs, there exists a minimum distance, equal to about $3/2a_0$ (8 Å), under which very few or no FP is found. Beyond this distance, the number of FPs increases dramatically and reaches a plateau at about $4a_0$ (22 Å), where very few FP are counted. This distance at which the curves kick off corresponds to the uranium FP of rank 4 and to the oxygen FP of rank 5. This result suggests that during collision cascades, fast FP recombinations take place as described in Secs. II and III, even if, in this case, numerous events occur at the same time. In cascades, the larger distance between the vacancy and the interstitial is not limited to $3/2a_0$. Moreover, the temperature during the collision sequence increases locally to very high temperature (up to the fusion point of 3200 K), which decreases the FP recombination times. Therefore, it seems that the threshold distance of $3/2a_0$ corresponds to the "thermal recombination distance" (r_{td}) defined above.

The role of the FP recombinations on the resistance to amorphization has also been investigated. It has been suggested by Chartier *et al.*[8,19] that the close FP recombination process plays a key role on the resistance to amorphization under irradiation in the lanthanum zirconate pyrochlore. This study has been carried out by accumulating FPs at different temperatures and different accumulation doses. Every 1 ps, a FP is introduced into the system, and then the system is relaxed under constant pressure and temperature. This time of 1 ps between each introduction of FP corresponds to the time under which instantaneous FP recombinations take place. More details about the method are described elsewhere.[19] They find for temperature under a certain threshold and for a certain dose that amorphization occurs in this pyrochlore. The same procedure has been applied to UO_2. Here amorphization is defined by the change on the radial pair-correlation function, where only the first coordination peak appears. Whatever the temperature (from 1 to 800 K) and the accumulation dose (up to ten displacements per cation), no amorphization has been found. This highlights the fact that FP recombination plays against the amorphization. One of the differences between both materials stems is that for UO_2, the total number of spontaneous cationic recombinations possible is equal to 30 (6 for rank 1 and 24 for rank 3), whereas in pyrochlore it is only 18 (6 for rank 1 and only 12 out of 24 of rank 3 are recombining).

V. CONCLUSIONS

MD simulations with empirical interatomic potential have been carried out to investigate the FP recombination mechanisms in the UO_2 fluorite matrix. The results show that for both uranium and oxygen FPs, the general picture of recombinations is rather complex. For the cations, the recombination is spontaneous for the FPs of ranks 1 and 3. The FP of rank 2 is found stable for the time scale of the simulation. For the FPs of rank 4, two different thermally activated recombinations are found. For the anions, the recombination is spontaneous for the FPs of ranks 1 and 2, and thermally activated for the FPs of ranks 3 to 5.

In our simulations, we found that the recombination mechanism can be seen as hops of the vacancy along certain crystallographic directions, until it reaches the spontaneous recombination distance. The lower recombination activation energies correspond to the migration paths along the [110] direction for the uranium FPs, and along the [100] direction for the oxygen FPs. In all the cases, the recombination activation energies are lower than the diffusion migration energies. The recombination process is of different nature than the classical thermal diffusion. The differences between the recombination activation energies are understood by the different migration paths. Further simulations describing more accurately the energies of the system, involving, for instance, DFT *ab initio*, will be necessary to confirm these behaviors.

Comparing the present results with those obtained with

previous MD simulations of displacement cascades, the "thermal recombination distance" is found to be equal to $3/2a_0$ for both uranium and oxygen FPs. Finally, accumulation of FPs does not show any amorphization of the fluorite matrix for any temperature contrary to what is found in lanthanum zirconate pyrochlore. This result enhanced the hypothesis, which considers that the fast FP recombinations play a key role in the resistance to amorphization.

*laurent.vanbrutzel@cea.fr

[1] H. J. Matzke and J. L. Whitton, Can. J. Phys. **44**, 995 (1966).
[2] J. P. Stout, G. R. Lumpkin, R. C. Ewing, and Y. Eyal, *Radiation Tolerance of Complex Oxide*, MRS Symposia Proceedings No. 112 (Materials Research Society, Pittsburgh, 1988), p. 495.
[3] M. Fayek, P. Burns, G. Yong-Xiang, and R. C. Ewing, J. Nucl. Mater. **277**, 204 (2000).
[4] K. Trachenko, J. Phys.: Condens. Matter **16**, R1491 (2004).
[5] L. W. Hobbs, Nucl. Instrum. Methods Phys. Res. B **91**, 30 (1994).
[6] K. E. Sickafus, R. Minervini, R. W. Grimes, J. A. Valdez, M. Ishimaru, F. Li, K. J. McClellan, and T. Hartmann, Science **289**, 748 (2000).
[7] J. Lian, L. M. Wang, and R. C. Ewing, J. Appl. Phys. **97**, 113536 (2005).
[8] A. Chartier, C. Meis, J.-P. Crocombette, W. J. Weber, and L. R. Corrales, Phys. Rev. Lett. **94**, 025505 (2005).
[9] L. Van Brutzel, M. Rarivomanantsoa, and D. Ghaleb, J. Nucl. Mater. **354**, 28 (2006).
[10] L. Van Brutzel and M. Rarivomanantsoa, J. Nucl. Mater. **358**, 209 (2006).
[11] E. Kotomin and V. Kuzovkov, Rep. Prog. Phys. **55**, 2079 (1992).
[12] J. Crocombette and A. Chartier, Nucl. Instrum. Methods Phys. Res. B **250**, 24 (2006).
[13] D. Morelon, N. D. Ghaleb, J. Delaye, and L. Van Brutzel, Philos. Mag. **83**, 1533 (2003).
[14] K. Govers, S. Lemehov, M. Hou, and M. Verwerft, J. Nucl. Mater. **366**, 161 (2007).
[15] J.-M. Delaye and D. Ghaleb, Nucl. Instrum. Methods Phys. Res. B **135**, 201 (1998).
[16] J. Durinck, M. Freyss, and P. Garicia, CEA-Cadarache Technical Report No. NT/SESC/LLCC-07-009, 2007 (unpublished).
[17] F. Gao and W. J. Weber, J. Appl. Phys. **94**, 4348 (2003).
[18] L. Malerba and J. M. Perlado, Phys. Rev. B **65**, 045202 (2002).
[19] J.-P. Crocombette, A. Chartier, and W. J. Weber, Appl. Phys. Lett. **88**, 051912 (2006).